

Uniform Circular Arrays in Near-Field: Omnidirectional Coverage with Limited Capacity

Ahmed Hussain, *Graduate Student Member, IEEE*, Asmaa Abdallah *Member, IEEE*,
Abdulkadir Celik, *Senior Member, IEEE*, and Ahmed M. Eltawil, *Senior Member, IEEE*

Abstract—Recent studies suggest that uniform circular arrays (UCAs) can extend the angular coverage of the radiative near-field region. This work investigates whether such enhanced angular coverage translates into improved spatial multiplexing performance when compared to uniform linear arrays (ULAs). To more accurately delineate the effective near-field region, we introduce the effective beamfocusing Rayleigh distance (EBRD)—an angle-dependent metric that bounds the spatial region where beamfocusing remains effective. Closed-form expressions for both beamdepth and EBRD are derived for UCAs. Our analysis shows that, under a fixed antenna element count, ULAs achieve narrower beamdepth and a longer EBRD than UCAs. Conversely, under a fixed aperture length, UCAs provide slightly narrower beamdepth and a marginally longer EBRD. Simulation results further confirm that ULAs achieve higher sum-rate under the fixed element constraint, while UCAs offer marginal performance gain under the fixed aperture constraint.

Index Terms—ULA, UCA, beamdepth, effective beamfocusing Rayleigh distance, UM-MIMO.

I. INTRODUCTION

WITH the success of massive multiple-input multiple-output (MIMO) technology in fifth generation (5G) systems, future wireless networks are expected to adopt ultra-massive (UM)-MIMO antenna arrays, along with the transition to higher frequency bands [1]. The deployment of large antenna arrays operating at high carrier frequencies shifts the communication paradigm from the far-field to the radiative near-field region. Extending beyond the reactive near-field up to the Rayleigh distance, the radiative near-field is characterized by spherical wavefronts, in contrast to the planar waves of the far-field. While far-field user equipments (UEs) can be served based solely on angular separation, the spherical nature of wave propagation in the near-field enables the formation of finite-depth beams. These beams allow UE separation in both angle and range dimensions, thereby enhancing spatial multiplexing gains.

Recent studies show that both the beamdepth and the limits of beamfocusing depend on the direction in which the beam is focused and the geometry of the antenna array [2]. For a uniform linear array (ULA), the beamdepth is smallest at boresight and increases toward endfire directions [3], suggesting that finite-depth beams—and hence near-field benefits—are confined primarily to UEs located near boresight. To overcome this restricted angular coverage, uniform circular arrays (UCAs) owing to their rotational symmetry, have been proposed to extend the near-field region [4]. This motivates a key question:

Does the omnidirectional coverage of the UCA translate into improved spatial multiplexing performance in the near-field?

UCAs are well-suited for direction-finding applications (e.g., RADAR) thanks to their uniform angular resolution, omnidirectional coverage, and immunity to scan loss. However, beamforming with UCAs presents notable challenges due to the complex synthesis of excitation weights, often requiring phase excitation modes [5]. In contrast to ULAs, which benefit from a Fourier transform relationship between the excitation weights and the far-field pattern, UCAs lack this structural simplicity. Specifically, the total radiation pattern of a UCA cannot be decomposed into a product of the element pattern and array factor. Moreover, in the far-field regime, the spatial multiplexing capability of UCAs is inherently limited: single-user capacity is degraded due to non-uniform singular values [6], while multi-user capacity is reduced due to correlated channels [7].

Existing studies to characterize and enhance the near-field region using UCAs have relied on the effective Rayleigh distance (ERD) metric [4]. The ERD identifies the near-field boundary where beamforming loss incurred while using far-field channel model exceeds a predefined threshold. However, the reported enhancement in angular coverage based on ERD in [4] assumes a fixed aperture length and neglects the elevation coverage intrinsic to UCAs. More critically, ERD is not directly related to near-field beamfocusing, which is fundamental for exploiting spatial multiplexing gains. Moreover, it is essential to evaluate the achievable communication capacity under practical system constraints, such as a fixed number of antenna elements or a constrained aperture length. To the best of the authors' knowledge, a rigorous comparison of the near-field multi-user capacity between UCA and ULA, remains unexplored in the literature.

To address these gaps, this work derives closed-form expressions for beamdepth and introduces the effective beamfocusing Rayleigh distance (EBRD) for the UCA. The EBRD serves as a metric that defines the boundary of the near-field region where beamfocusing remains effective. A comparative analysis of beamdepth and EBRD is carried out for both ULA and UCA under two practical design constraints: fixed antenna element count and fixed aperture length. Furthermore, simulation results are presented to compare the multi-user capacity of these array configurations under the same constraints.

II. SYSTEM MODEL

We consider the downlink of a single-cell multi-user UM-MIMO system, where a base station (BS) with N_{BS} antennas

The authors are with Computer, Electrical, and Mathematical Sciences and Engineering (CEMSE) Division, King Abdullah University of Science and Technology (KAUST), Thuwal, 23955-6900, KSA.

simultaneously communicates with K single-antenna UEs within its coverage area. The received signal at the k^{th} UE can be expressed as

$$y_k = \sqrt{\gamma} \mathbf{w}_k \mathbf{h}_k s_k + \sqrt{\gamma} \sum_{j=1, j \neq k}^K \mathbf{w}_j \mathbf{h}_k s_j + z_k, \quad (1)$$

where $\gamma = \frac{P}{N_{\text{BS}}}$ is the average signal-to-noise ratio (SNR), P is the total transmit power, s_k and s_j are the transmit symbols with unit-norm, $\mathbf{w}_k \in \mathbb{C}^{1 \times N_{\text{BS}}}$ and $\mathbf{w}_j \in \mathbb{C}^{1 \times N_{\text{BS}}}$ are unit norm precoding vectors for UE k and j , respectively, and $z_k \sim \mathcal{CN}(0, 1)$ denotes the zero-mean complex Gaussian additive noise. $\mathbf{h}_k \in \mathbb{C}^{N_{\text{BS}} \times 1}$ is the near-field channel vector between the BS and the k^{th} UE which is given by

$$\mathbf{h}_k = \beta_k \mathbf{b}(r_k, \theta_k, \varphi_k), \quad (2)$$

where β_k represents the complex path gain associated with the line-of-sight (LoS) propagation path of UE k , while $\mathbf{b} \in \mathbb{C}^{N_{\text{BS}} \times 1}$ denotes the near-field array response vector that is focused at a specific range r_k , elevation angle θ_k , and azimuth angle φ_k . At millimeter wave (mmWave) frequencies, LoS path is at least 4–5 dB greater compared to other multipath components [7]. Therefore, herein we focus on the LoS path, and assume $\beta_k = 1$.

A. Achievable Rate

The achievable rate for the k^{th} UE can be expressed as [7]

$$\mathcal{R}_k = \log_2(1 + \text{SINR}_k), \quad (3)$$

where

$$\text{SINR}_k = \frac{\gamma |\mathbf{w}_k \mathbf{h}_k|^2}{1 + \gamma \sum_{j=1, j \neq k}^K |\mathbf{w}_j \mathbf{h}_k|^2}. \quad (4)$$

Based on (3), the achievable sum-rate will be $R_{\text{sum}} = \sum_{k=1}^K \mathcal{R}_k$. We assume that perfect channel state information is available at the BS. Assuming maximum ratio transmission, the precoding vector \mathbf{w}_k is given by $\mathbf{w}_k = \mathbf{h}_k^H / \sqrt{N_{\text{BS}}}$. Accordingly, the achievable sum-rate in (3) can then be written as

$$\mathcal{R}_k = \log_2 \left(1 + \frac{\gamma N_{\text{BS}}}{1 + \gamma N_{\text{BS}} \sum_{j=1, j \neq k}^K \mathcal{G}_{a,kj}^2} \right), \quad (5)$$

where $\mathcal{G}_{a,kj}$ denotes the value of the inner product of \mathbf{h}_k and \mathbf{h}_j , which is defined as

$$\mathcal{G}_{a,kj} = \frac{|\mathbf{h}_k^H(r_k, \theta_k, \varphi_k) \mathbf{h}_j(r_j, \theta_j, \varphi_j)|}{N_{\text{BS}}}. \quad (6)$$

The symbol $a \in [\text{ula}, \text{uca}]$ denotes the array configuration, such as ULA or UCA. As evident from (5), the term $\mathcal{G}_{a,kj}$ plays a critical role in determining the achievable sum-rate. Specifically, minimizing the summation $\sum_{j=1, j \neq k}^K \mathcal{G}_{a,kj}^2$ reduces inter-user interference and leads to improved rate performance, whereas larger values of this term degrades the achievable sum-rate. Furthermore, (6) can be analyzed in both the angular and range domains. While the angular-domain behavior remains consistent across the near-field and far-field regimes, the range-domain characteristics vary considerably. In the subsequent sections, we analyze the behavior of $\mathcal{G}_{a,kj}$ in the range domain for both ULA and UCA configurations.

B. Channel Model

We consider a UCA as depicted in Fig. 1, where antenna elements are uniformly distributed along the circle of radius R . The UE is located at a distance r from the center of the UCA and subtends elevation angle θ and azimuth angle φ . In

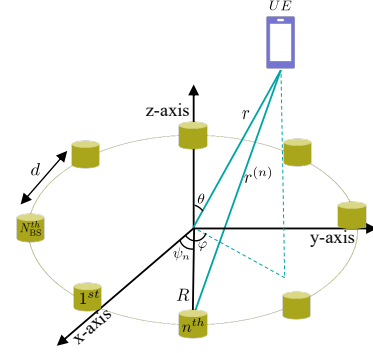


Fig. 1: UCA for near-field communication system.

polar coordinates, the geometrical position of each antenna element is represented as (R, ψ_n) , where $\psi_n = \frac{2\pi n}{N_{\text{BS}}}$ for $n \in [1, 2, \dots, N_{\text{BS}}]$. As the number of antennas in UM-MIMO increases, the far-field planar wave propagation model becomes inaccurate and a spherical-wave model must be employed to accurately characterize the wave propagation. Traditionally, the Rayleigh distance, $r_{\text{RD}} = \frac{2D^2}{\lambda}$, is defined as the boundary separating the radiative near-field and far-field regions, where D denotes the aperture length and λ represents the wavelength. In this paper, the minimum distance from the BS in the radiative near-field is set as $1.2D$ such that amplitude variations across the array are negligible, and accordingly, a uniform spherical wave (USW) is employed. Correspondingly, the near-field array response vector is formulated as

$$\mathbf{b}(r, \theta, \varphi) = \frac{1}{\sqrt{N_{\text{BS}}}} \left[e^{-j \frac{2\pi}{\lambda} (r^{(1)} - r)}, \dots, e^{-j \frac{2\pi}{\lambda} (r^{(N_{\text{BS}})} - r)} \right]^T, \quad (7)$$

where $r^{(n)}$ denotes the propagation distance between the UE and the n^{th} antenna of the UCA. From Fig. 1, based on the law of cosines, $r^{(n)} = \sqrt{r^2 + R^2 - 2rR \sin \theta \cos(\varphi - \psi_n)}$, which can be further approximated using the second-order Taylor series expansion as

$$r^{(n)} \approx r - R \sin \theta \cos(\varphi - \psi_n) + \frac{R^2}{2r} (1 - \sin^2 \theta \cos^2(\varphi - \psi_n)) \quad (8)$$

III. ANALYSIS OF UCA NEAR-FIELD BEAMFORMING

In this section, we formulate array gain in the distance dimension, based on which we derive closed form expressions for the beamdepth and EBRD for UCAs.

A. Array Gain

Far-field beams exhibit finite beamwidth and infinite beamdepth, while near-field beams focus energy in both angle and range with finite beamwidth and beamdepth, respectively. Finite-depth beamforming is achieved in the radiative near-field through the conventional matched filtering approach, where the phase of each radiating source is set to compensate for the path difference between the focal point r_f and the source to achieve constructive interference at the focal point. Suppose we focus the beam at r_f ; the array gain at varying distances $r \in [1.2D, \infty]$, but same azimuth φ and elevation angle θ , is given by

$$\mathcal{G}_{\text{uca}} = |\mathbf{w}(r, \theta, \varphi) \mathbf{b}(r_f, \theta, \varphi)|, \quad (9)$$

where $\mathbf{w}(r, \theta, \varphi)$ is the beamforming vector.

Theorem 1. The normalized array gain obtained by near-field beamforming for a UCA can be approximated as follows

$$\mathcal{G}_{\text{uca}} = \frac{1}{N_{\text{BS}}} \left| \sum_{n=1}^{N_{\text{BS}}} e^{j \frac{2\pi}{\lambda} \left\{ \frac{R^2}{2} r_{\text{eff}} (1 - \sin^2 \theta \cos^2(\varphi - \psi_n)) \right\}} \right| \approx |J_0(\zeta)| \quad (10)$$

where $\zeta = \frac{\pi r_{\text{RD}}^{\text{uca}}}{16} r_{\text{eff}} \sin^2 \theta$ and $r_{\text{eff}} = \left| \frac{r - r_F}{r r_F} \right|$.

Proof. The proof is provided in **Appendix A**. \square

B. Beamdepth

We define the beamdepth r_{BD} as the distance interval $r \in [r_{\text{F}}^{\text{min}}, r_{\text{F}}^{\text{max}}]$ where normalized array gain \mathcal{G}_{uca} is at most 3 dB lower than its maximum value.

Corollary 1. For a UCA, the beamdepth $r_{\text{BD}}^{\text{uca}}$ obtained by focusing a beam at a distance r_F from the BS is given by

$$r_{\text{BD}}^{\text{uca}} = \begin{cases} \frac{32\pi r_{\text{RD}}^{\text{uca}} r_F^2 \sin^2 \theta}{(\pi r_{\text{RD}}^{\text{uca}} \sin^2 \theta)^2 - (16r_F \alpha_{3\text{dB}})^2}, & r_F < \frac{\pi r_{\text{RD}}^{\text{uca}}}{16\alpha_{3\text{dB}}} \sin^2 \theta \\ \infty, & r_F \geq \frac{\pi r_{\text{RD}}^{\text{uca}}}{16\alpha_{3\text{dB}}} \sin^2 \theta \end{cases} \quad (11)$$

Proof. The proof is provided in **Appendix B**. \square

Note that although $r_{\text{BD}}^{\text{uca}}$ in (11) is independent of azimuth angle φ , it depends on the elevation angle θ . Furthermore, $r_{\text{BD}}^{\text{uca}}$ increases as the focus distance r_F increases or elevation angle moves towards the boresight direction ($\theta = 0^\circ$).

C. Effective Beamfocusing Rayleigh Distance (EBRD)

Finite depth beams are achieved in the near-field, only when the focus distance r_F lies within a certain range limit for a given elevation angle θ in (11). We derive this limit for a UCA and refer to it as EBRD.

Corollary 2. The farthest distance at which near-field beamfocusing for a UCA can be achieved is bounded by $r_F < \frac{\pi r_{\text{RD}}^{\text{uca}}}{16\alpha_{3\text{dB}}} \sin^2 \theta$.

Proof. The proof is provided in **Appendix C**. \square

EBRD is minimum in the boresight direction ($\theta = 0^\circ$) and increases at end-fire directions ($\theta = \pm 90^\circ$).

IV. COMPARATIVE ANALYSIS WITH ULA

In this section, we investigate the beamdepth and the EBRD to characterize spatial correlation in the range domain for both ULA and UCA. Note that \mathcal{G}_{uca} in (9) can also be interpreted as spatial correlation between near-field UEs located at ranges r and r_F , respectively.

A. Beamdepth and EBRD

A narrow beamdepth and extended EBRD facilitate reduced inter-user interference, thereby enhancing spatial multiplexing. By definition of the beamdepth, the spatial correlation satisfies $\mathcal{G}_{\text{uca}} > 0.5$ between a UE located at range r_F and other UEs within the interval $r \in [r_{\text{F}}^{\text{min}}, r_{\text{F}}^{\text{max}}]$. For UEs outside this region, $\mathcal{G}_{\text{uca}} < 0.5$, governed by the forelobe behavior of the gain pattern. In this subsection, we compare spatial correlation of the ULA and UCA in terms of beamdepth and forelobes under the constraint of fixed antenna element count and fixed aperture length. First, we compare the aperture lengths of the arrays under the constraint of equal antenna element count.

Theorem 2. For equal antenna count, the UCA has an aperture length reduced by a factor of π relative to the ULA.

Proof. For N_{BS} antenna elements, the aperture length of a ULA is $D_{\text{ula}} \approx N_{\text{BS}} d$. In contrast, the antenna elements in a UCA are placed on a circle of circumference $\pi D_{\text{uca}} = N_{\text{BS}} d$, resulting in an effective aperture length of $D_{\text{uca}} = \frac{N_{\text{BS}} d}{\pi}$. Therefore,

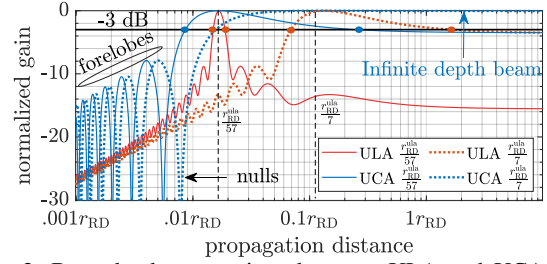


Fig. 2: Beamdepth comparison between ULA and UCA for fixed $N_{\text{BS}} = 256$, $f_c = 28$ GHz. Here $r_{\text{RD}} = r_{\text{ula}}^{\text{ula}} = 348$ m.

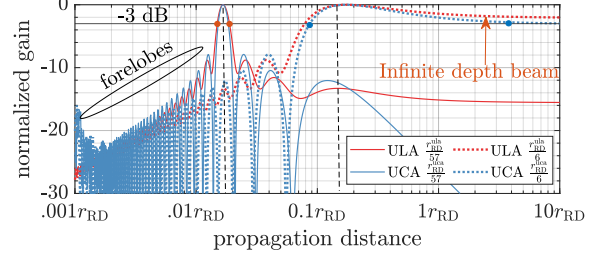


Fig. 3: Beamdepth comparison between ULA and UCA for fixed aperture length of 1.36 m at $f_c = 28$ GHz. Here $r_{\text{RD}} = r_{\text{ula}}^{\text{ula}} = r_{\text{uca}}^{\text{uca}}$.

$D_{\text{uca}} = \frac{D_{\text{ula}}}{\pi}$, which completes the proof. Also $r_{\text{RD}}^{\text{uca}} = \frac{2D_{\text{ula}}^2}{\lambda}$, exceeds $r_{\text{RD}}^{\text{ula}} = \frac{2D_{\text{uca}}^2}{\lambda}$ by a factor of π^2 . \square

The beamdepth $r_{\text{BD}}^{\text{ula}}$ and the corresponding EBRD for a ULA are given by [3]

$$r_{\text{BD}}^{\text{ula}} = \begin{cases} \frac{8\alpha_{3\text{dB}} r_F^2 r_{\text{RD}}^{\text{ula}} \cos^2(\varphi)}{(r_{\text{RD}}^{\text{ula}} \cos^2(\varphi))^2 - (4\alpha_{3\text{dB}} r_F)^2}, & r_F < \frac{r_{\text{RD}}^{\text{ula}}}{4\alpha_{3\text{dB}}} \cos^2(\varphi) \\ \infty, & r_F \geq \frac{r_{\text{RD}}^{\text{ula}}}{4\alpha_{3\text{dB}}} \cos^2(\varphi) \end{cases} \quad (12)$$

Notably, the EBRD for a ULA is maximized in the boresight direction, i.e., at $\varphi = 0^\circ$ in (12), whereas the UCA exhibits its minimum EBRD at $\theta = 0^\circ$ (boresight direction), as given in Corollary 2. Consequently, UEs located at the boresight of the UCA or in the endfire direction of the ULA may not fully benefit from near-field beamfocusing. Note that the rotational symmetry of a UCA is confined to the azimuth plane and does not extend to the elevation dimension. Consequently, the beamfocusing characteristics of a UCA remain invariant with respect to the azimuth angle but are dependent on the elevation angle.

1) Fixed Number of Antenna Elements

Under a fixed antenna count N_{BS} , the ULA achieves a narrower beamdepth and a more extended EBRD compared to the UCA. When comparing beamdepth at the same focus distance, r_{RD} is the only significant geometry-dependent parameter in (11) and (12). Both expressions indicate that beamdepth decreases with increasing r_{RD} . As stated in Theorem 2, since $D_{\text{ula}} > D_{\text{uca}}$, it follows that $r_{\text{RD}}^{\text{ula}} > r_{\text{RD}}^{\text{uca}}$, leading to a narrower beamdepth for the ULA compared to the UCA.

To further illustrate this, Fig. 2 shows the normalized array gain as a function of propagation distance. The distance interval between the 3 dB gain points defines the beamdepth. For a fair comparison, we choose $\theta = 90^\circ$ for the UCA and $\varphi = 0^\circ$ for the ULA, as these angles minimize the beamdepth according to (11) and (12), respectively. When focusing the beam at a near-field distance of $r_F = r_{\text{RD}}^{\text{ula}}/57$, the ULA achieves a significantly narrow beamdepth of 1.4 m, compared to 84 m for the UCA. Here $r_{\text{RD}}^{\text{ula}} = 348$ m and $r_{\text{RD}}^{\text{uca}} = 35$ m. Furthermore, ULA achieves

TABLE I: Array gain in angle and range domains.

Array	Angle Domain [4], [7]	Range Domain [3], (10)
ULA	$\text{sinc}\left(\frac{N_{\text{BS}}d}{\lambda}(\sin\varphi_j - \sin\varphi_k)\right)$	$\frac{C(\gamma) + jS(\gamma)}{\gamma}$
UCA	$J_0\left(\frac{4\pi R}{\lambda}\sin\left(\frac{\varphi_j - \varphi_k}{2}\right)\right)$	$J_0\left(\frac{\pi R^2}{2\lambda}r_{\text{eff}}\sin^2\theta\right)$

finite depth beams up till (EBRD) $r_{\text{RD}}^{\text{ula}}/7 = 49.7\text{ m}$; the same limit is also obtained from (12), where $\alpha_{3\text{dB}} = 1.75$ for $\varphi = 0^\circ$. On the other hand EBRD for UCA is only $r_{\text{RD}}^{\text{ula}}/57 = r_{\text{RD}}^{\text{uca}}/6 \approx 6\text{ m}$. As shown in Fig. 2, ULA maintains a finite beamdepth up to $r_{\text{RD}}^{\text{ula}}/7$, while it becomes infinite for UCA highlighted by the dotted blue line for UCA at $r_{\text{RD}}^{\text{ula}}/7$, which stays above the 3 dB threshold beyond the focusing point.

Fig. 2 also illustrates the spatial correlation between a UE located at the focal point r_{F} and UEs positioned outside the interval $r \in [r_{\text{F}}^{\text{min}}, r_{\text{F}}^{\text{max}}]$. Notably, the forelobes of the UCA exceed those of the ULA by approximately 8–10 dB, indicating higher spatial correlation for UCA between the UE at r_{F} and UEs outside the beamdepth region. This elevated correlation may adversely impact the capacity performance of the UCA. Conversely, the UCA can form nulls in the spatial correlation pattern, which is not achievable with the ULA, as also shown in Fig. 2. Nevertheless, in practical deployments, UE locations are random and cannot be controlled to align with these null positions.

2) Fixed Aperture Length

For a fixed aperture length, the UCA demonstrates a slightly narrower beamdepth and a marginally larger EBRD compared to the ULA. Achieving equal aperture lengths for both array configurations in Fig. 3 requires a significantly higher number of antenna elements for the UCA. For instance, at a carrier frequency of 28 GHz, matching aperture lengths of 1.36 m necessitates 256 elements for the ULA, whereas the UCA requires 801 elements. In this case, $D_{\text{ula}} = D_{\text{uca}}$ implies $r_{\text{RD}}^{\text{ula}} = r_{\text{RD}}^{\text{uca}}$, and the slightly narrower beamdepth for the UCA in (11) compared to ULA in (12) arises from differences in $\alpha_{3\text{dB}}$ and constant factors.

As shown in Fig. 3, when the beam is focused at $r_{\text{RD}}^{\text{ula}}/57$, the UCA achieves a slightly narrower beamdepth compared to the ULA. In the boresight scenario, the EBRD of the UCA is approximately $r_{\text{RD}}^{\text{uca}}/6$, which slightly exceeds that of the ULA, $r_{\text{RD}}^{\text{ula}}/7$. The EBRD for UCA can also be derived directly from Corollary 2, using $\alpha_{3\text{dB}} = 1.2$. At $r_{\text{RD}}^{\text{uca}}/6$, the UCA maintains a well-defined finite-depth beam, whereas the ULA exhibits an infinite-depth beam—evident from the trailing edge at $r_{\text{RD}}^{\text{ula}}/6$ (red dotted curve) remaining above the 0.5 gain threshold. Additionally, despite having the same aperture length, the forelobes of the UCA exceed those of the ULA by approximately 1–2 dB across all ranges. As a result, the UCA exhibits stronger spatial correlation between a UE at r_{F} and surrounding UEs outside the beamdepth region.

B. Asymptotic Orthogonality

Channels \mathbf{h}_k and \mathbf{h}_j are asymptotically orthogonal if $\lim_{N_{\text{BS}} \rightarrow \infty} \frac{|\mathbf{h}_k^H \mathbf{h}_j|}{N_{\text{BS}}} \rightarrow 0$. Closed-form expressions for $\mathcal{G}_{*,jk}$ in both angular and range domains are summarized in Table I.

For a ULA, the range-domain array gain is given by $\mathcal{G}_{\text{ula}} = \left| \frac{C(\gamma) + jS(\gamma)}{\gamma} \right|$, where $\gamma = \sqrt{\frac{N_{\text{BS}}^2 d^2 \cos^2(\varphi)}{2\lambda}} r_{\text{eff}}$, and

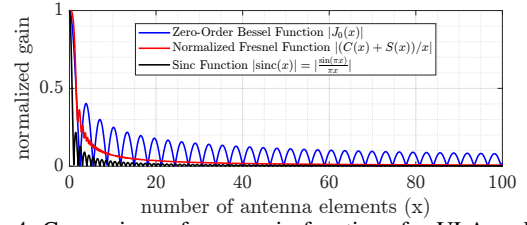


Fig. 4: Comparison of array gain functions for ULA vs UCA.

$C(\gamma)$ and $S(\gamma)$ denote the Fresnel cosine and sine integrals, respectively [3]. In the limit as $N_{\text{BS}} \rightarrow \infty$, $\gamma \rightarrow \infty$, and using the property $C(\infty) = S(\infty) = 0.5$, it follows that $\mathcal{G}_{\text{ula}} \rightarrow 0$.

For a UCA, the array gain in the range domain is characterized by the zero-order Bessel function $J_0(\zeta)$ as shown in (10). The asymptotic form $J_0(\zeta) \sim \sqrt{\frac{2}{\pi\zeta}} \cos\left(\zeta - \frac{\pi}{4}\right)$ [8] implies $J_0(\zeta) \rightarrow 0$ as $\zeta \rightarrow \infty$. Since ζ is proportional to the array radius R , increasing N_{BS} increases R and consequently ζ , ensuring $\mathcal{G}_{\text{uca},jk} \rightarrow 0$ for UCA as well.

As summarized in Table I, the angular-domain array gain for the ULA is governed by the sinc function [7], while for the UCA, it is defined by the Bessel function [4]. The asymptotic orthogonality of both array types in angular and range domains is established in the literature. For further comparison, Fig. 4 illustrates the decay behavior of these array gain functions, with x denoting a scaled variable proportional to N_{BS} .

While both ULA and UCA achieve asymptotic orthogonality, their array gain functions exhibit distinct decay profiles: the sinc and Fresnel integrals decay monotonically as $1/x$, whereas the Bessel function decays as $1/\sqrt{x}$ with oscillatory behavior. Consequently, for a given N_{BS} , the sinc function yields the lowest correlation, followed by the Fresnel and Bessel functions. This indicates that ULA multiplexes a higher number of UEs in the angular domain, followed by its range domain, and then by the range/angle domain of the UCA.

V. SIMULATION RESULTS

In this section, we conduct Monte Carlo simulations to evaluate and compare the achievable sum-rate in (5) for both UCA and ULA, under constraints of fixed number of antenna elements and fixed aperture length.

A. Fixed Number of Antenna Elements

In this scenario, both UCA and ULA are configured with $N_{\text{BS}} = 256$ at a carrier frequency of 28 GHz. For this value of N_{BS} , the resulting aperture lengths are 0.43 m for the UCA and 1.3 m for the ULA. Consequently, the corresponding Rayleigh distances are approximately 35 m and 348 m for the UCA and ULA, respectively. For each array configuration, 50 UEs are randomly placed within the range interval $[1.2D, \text{EBRD}]$.

Fig. 5 presents the achievable sum-rate with respect to SNR for both array geometries. It is observed that the ULA consistently outperforms the UCA across all SNR regimes. This performance gap can be attributed to the reduced beamdepth, extended EBRD and reduced spatial correlation as explained in Sec. IV-A1. Furthermore, we evaluate the UCA under three different UE distribution scenarios. In the first case, UEs are uniformly distributed across both azimuth and elevation, i.e., $\theta \sim \mathcal{U}[-\pi/2, \pi/2]$, $\varphi \sim \mathcal{U}[-\pi, \pi]$. This configuration yields the highest sum-rate, as the spatial decorrelation between UEs is maximized in the 2D domain. Conversely, the lowest

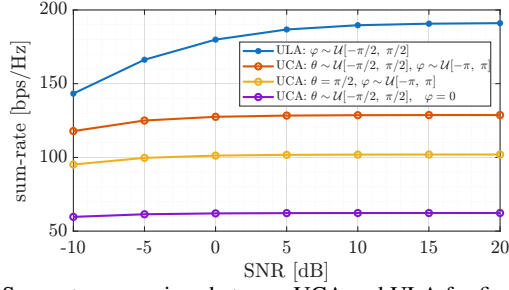


Fig. 5: Sum-rate comparison between UCA and ULA for fixed antenna element count, $N_{BS} = 256$.

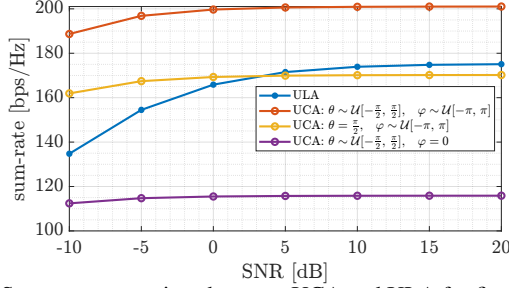


Fig. 6: Sum-rate comparison between UCA and ULA for fixed aperture length, $D_{ula} = D_{ua} = 1.36$ m.

sum-rate is observed when UEs are distributed only in the elevation dimension. This behavior is due to the elevation dependence of both the beamdepth and the EBRD; specifically, the beamdepth becomes infinite at the boresight in the elevation plane. The intermediate case corresponds to a fixed elevation angle $\theta = \pi/2$ with UEs uniformly distributed in azimuth, i.e., $\varphi \sim \mathcal{U}[-\pi, \pi]$. In this case, the beamdepth is narrowest and invariant with respect to the azimuth angle.

B. Fixed Aperture Length

Fig. 6 compares the sum-rate under a fixed aperture length of 1.36 m. When UEs are distributed across both azimuth and elevation, the UCA outperforms the ULA, primarily due to its two-dimensional geometry, which spans a larger area and increases the likelihood of reduced spatial correlation. However, when UEs are confined to the azimuth plane, the performance gap narrows, and the ULA achieves higher sum-rate compared to the UCA, especially at high SNR. In contrast, when UEs are distributed solely in the elevation plane, the ULA consistently outperforms the UCA. Although the beamdepth and EBRD are comparable, as shown in Fig. 3, the UCA exhibits higher spatial correlation outside the beamdepth region, resulting in degraded performance in the 1D case.

VI. CONCLUSION

In this paper, we compared the spatial correlation between UEs for ULA and UCA configurations. Our results indicate that the capacity performance of the UCA is limited due to high spatial correlation, despite the 2D array geometry. Transitioning from uniform circular to concentric circular array may offer improved performance, as the latter exhibits lower forelobe levels in the angular domain. As a direction for future work, it would be interesting to analyze and compare the spatial correlation and corresponding capacity of uniform rectangular arrays and uniform concentric circular arrays in the near-field.

REFERENCES

- [1] W. Jiang, B. Han, M. A. Habibi, and H. D. Schotten, "The road towards 6G: A comprehensive survey," *IEEE Open J. Commun. Soc.*, vol. 2, pp.

- 334–366, Feb. 2021.
- [2] A. Abdallah, A. Hussain, A. Celik, and A. M. Eltawil, "Exploring frontiers of polar-domain codebooks for near-field channel estimation and beam training: A comprehensive analysis, case studies, and implications for 6G," *IEEE Signal Process. Mag.*, vol. 42, no. 1, pp. 45–59, 2025.
- [3] A. Hussain, A. Abdallah, and A. M. Eltawil, "Redefining polar boundaries for near-field channel estimation for ultra-massive MIMO antenna array," *IEEE Trans. Wireless Commun.*, pp. 1–1, 2025.
- [4] Z. Wu, M. Cui, and L. Dai, "Enabling more users to benefit from near-field communications: From linear to circular array," *IEEE Trans. Wireless Commun.*, vol. 23, no. 4, pp. 3735–3748, 2024.
- [5] R. Mital, M. P. Parent, and A. Stumme, "Circular array beamforming using phase modes," *Naval Research Lab, Washington, DC*, 2019.
- [6] P. Wang, Y. Li, and B. Vucetic, "Millimeter wave communications with symmetric uniform circular antenna arrays," *IEEE Commun. Lett.*, vol. 18, no. 8, pp. 1307–1310, 2014.
- [7] W. Tan, S. Jin, J. Wang, and Y. Huang, "Achievable sum-rate analysis for massive MIMO systems with different array configurations," in *IEEE Wireless Commun. Netw. Conf. (WCNC)*, 2015, pp. 316–321.
- [8] F. W. Olver, "The asymptotic expansion of bessel functions of large order," *Philos. Trans. R. Soc. Lond. A*, vol. 247, no. 930, pp. 328–368, 1954.

APPENDIX A

PROOF OF THEOREM 1

Utilizing (7) and (9), the array gain in the range domain for UCA is given by $\mathcal{G}_{uca} = \frac{1}{N_{BS}} \left| \sum_{n=1}^{N_{BS}} e^{j \frac{2\pi}{\lambda} \left(\frac{R^2}{2} r_{eff}^2 (1 - \sin^2 \theta \cos^2(\varphi - \psi_n)) \right)} \right|$, where $r_{eff} = \left| \frac{r - r_F}{r r_F} \right|$. Defining $\zeta = \frac{\pi}{\lambda} \frac{R^2}{2} r_{eff}^2 \sin^2 \theta$, substituting $R = D_{uca}/2$ and $r_{RD}^{uca} = \frac{2D_{uca}^2}{\lambda}$ yields $\zeta = \frac{\pi r_{RD}^{uca}}{16} r_{eff}^2 \sin^2 \theta$. Without loss of generality, let $\varphi = 0$ due to rotational symmetry of UCA, so $\mathcal{G}_{uca} \approx \frac{1}{N_{BS}} \left| \sum_{n=1}^{N_{BS}} e^{-2j\zeta \cos^2(\psi_n)} \right|$. Using trigonometric identity $\cos(2x) = 2\cos^2(x) - 1$, the gain simplifies to $\mathcal{G}_{uca} \approx \frac{1}{N_{BS}} \left| \sum_{n=1}^{N_{BS}} e^{-j\zeta \cos(2\psi_n)} \right|$. For large N_{BS} , this sum approximates the integral $\frac{1}{2\pi} \int_0^{2\pi} e^{-j\zeta \cos(\psi_n)} d\psi_n = J_0(\zeta)$, where $J_0(\zeta)$ is the Bessel function of the first kind and order zero. Hence, $\mathcal{G}_{uca} \approx |J_0(\zeta)|$, which completes the proof.

APPENDIX B

PROOF OF COROLLARY 1

To obtain the range points where the gain function in (10) equals 3 dB of its maximum value, we define $\alpha_{3dB} \triangleq \left\{ \zeta \mid |\mathcal{G}_{uca}(\zeta)|^2 = 0.5 \right\}$. Thus, $\alpha_{3dB} = \frac{\pi r_{RD}^{uca}}{16} r_{eff}^2 \sin^2 \theta$, where $r_{eff} = \left| \frac{r - r_F}{r r_F} \right|$. Solving for r yields two solutions: $r = \frac{\pi r_{RD}^{uca} \sin^2 \theta r_F}{\pi r_{RD}^{uca} \sin^2 \theta \pm 16\alpha_{3dB} r_F}$. Therefore, $r_F^{\max} = \frac{\pi r_{RD}^{uca} \sin^2 \theta r_F}{\pi r_{RD}^{uca} \sin^2 \theta - 16\alpha_{3dB} r_F}$, and $r_F^{\min} = \frac{\pi r_{RD}^{uca} \sin^2 \theta r_F}{\pi r_{RD}^{uca} \sin^2 \theta + 16\alpha_{3dB} r_F}$. The distance window between r_F^{\max} and r_F^{\min} is the interval where \mathcal{G}_{uca} is less than or equal to 3 dB. Therefore, $r_{BD} = r_F^{\max} - r_F^{\min}$ is given by (11), which completes the proof.

APPENDIX C

PROOF OF COROLLARY 2

In Theorem (1), the maximum value of r_{BD}^{uca} is obtained when the factor in the denominator $(\pi r_{RD}^{uca} \sin^2 \theta)^2 - (16r_F \alpha_{3dB})^2 = 0$. Thus, the farthest angle-dependent axial distance r_F , where we can have finite depth beamforming is less than $\frac{\pi r_{RD}^{uca}}{16\alpha_{3dB}} \sin^2(\theta)$.